

Safety-Critical Control for Aerial Physical Interaction in Uncertain Environment

Jeonghyun Byun¹, Yeonjoon Kim¹, Dongjae Lee¹, and H. Jin Kim¹

Abstract—Aerial manipulation for safe physical interaction with their environments is gaining significant momentum in robotics research. In this paper, we present a disturbance-observer-based safety-critical control for a fully actuated aerial manipulator interacting with both static and dynamic structures. Our approach centers on a safety filter that dynamically adjusts the desired trajectory of the vehicle’s pose, accounting for the aerial manipulator’s dynamics, the disturbance observer’s structure, and motor thrust limits. We provide rigorous proof that the proposed safety filter ensures the forward invariance of the safety set—representing motor thrust limits—even in the presence of disturbance estimation errors. To demonstrate the superiority of our method over existing control strategies for aerial physical interaction, we perform comparative experiments involving complex tasks, such as pushing against a static structure and pulling a plug firmly attached to an electric socket. Furthermore, to highlight its repeatability in scenarios with sudden dynamic changes, we perform repeated tests of pushing a movable cart and extracting a plug from a socket. These experiments confirm that our method not only outperforms existing methods but also excels in handling tasks with rapid dynamic variations.

I. INTRODUCTION

Aerial manipulators have gained popularity in robotics research due to their ability to combine the maneuverability of unmanned aerial vehicles (UAVs) with the versatility of robotic manipulators. Their capability to physically interact with the environment makes them ideal for a wide range of applications involving physical interaction such as drawer-opening [1], door-opening [2], plug-pulling [3], window-cleaning [4], multi-manual object manipulation [5], non-destructive testing (NDT) [6] and heavy object pushing [7].

Such tasks, often referred to as aerial physical interaction (APhI) depicted in Fig. 1, require consideration of two important factors when designing controllers. The first is the external disturbance generated by the physical interaction between the vehicle and the surrounding environment, and the second is the vehicle’s actuation limit such as motor thrust limit. However, very few studies have focused on controller design for APhI that simultaneously accounts for both disturbance attenuation and actuator limitations.

In [8], the control of a fully actuated UAV with actuator saturation was introduced, and in [9], the authors presented an actuator limit-aware control strategy for an aerial manipulator physically interacting with a human operator. However, they did not consider the effect of external disturbances

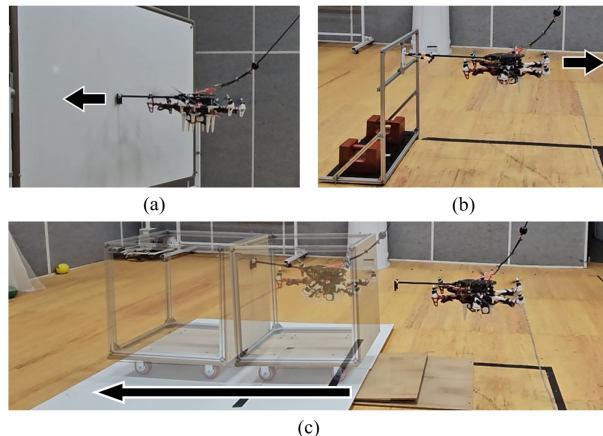


Fig. 1. Aerial physical interaction (APhI) experiments conducted for the validation of the proposed method. (a) Pushing a static structure. (b) Pulling an object from a static structure. (c) Pushing a movable object.

or model uncertainties when designing their controllers and only conducted numerical simulations.

In [10] and [11], energy tank-based controllers for aerial manipulators interacting with uncertain dynamic environments were presented. They proved the vehicle’s safety under the effect of external disturbances or model uncertainties. Also, [12] proposed a power-based safety layer for aerial vehicles physically interacting with surrounding environments, and [13] introduced a control method for human-robot APhI that considers motor thrust limitations and external disturbances. However, these four controllers assume that the interaction wrench can be measured by a force/torque sensor or estimated based on a derived model. This reliance may not be suitable for aerial manipulators not equipped with force/torque operating in windy environments.

[14] presented a saturated robust controller for a fully actuated multirotor taking into account the disturbance rejection and rotor thrust saturation. However, they did not consider the situation that reaching the desired pose of the vehicle is not dynamically feasible, e.g., the magnitude of an external disturbance exceeds the motor thrust limit, and only conducted numerical simulations.

In this paper, we present a disturbance-observer (DOB)-based safety-critical control of a fully actuated aerial manipulator physically interacting with static or movable structures. To that end, we derive the dynamic model of the aerial manipulator configured with a fully actuated hexacopter and a rigidly attached robotic arm. Then, the control framework including a DOB-based control law and a safety filter is

¹ The authors are with the Department of Aerospace Engineering, Automation and System Research Institute(ASRI) and Institute of Advanced Aerospace Technology(IAAT), Seoul National University, Seoul, South Korea. {quswjdqus97, 0831joon, ehdwo713, hjinkim}@snu.ac.kr

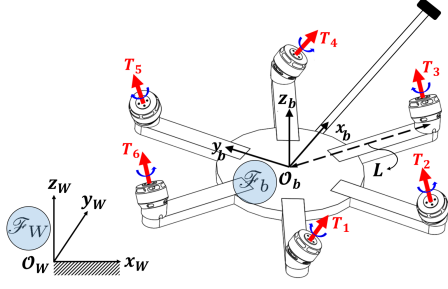


Fig. 2. An aerial manipulator configured with a fully actuated multirotor and a rigidly attached robotic arm. The thrust values T_1, \dots, T_6 configure the thrust vector $\mathbf{T} \in \mathbb{R}^6$, and \mathcal{F}_W and \mathcal{F}_b represent the Earth-fixed and multirotor frames, respectively.

introduced. While the DOB-based control law is designed as presented in [15], for the safety filter, we develop a system model that combines the aerial manipulator's model and DOB structure and formulate an optimization problem to determine the desired pose and twist of the vehicle that conforms to the constraints on motor thrust. In particular, our main contributions are arranged as follows:

- We design a safety-critical controller that can conduct various types of APhI with uncertain environments in the absence of interaction wrench measurement or estimation.
- We show that the safety set representing the motor thrust limits is forward invariant under the proposed safety filter.
- We validate that our controller outperforms existing approaches for APhI control through pushing and pulling experiments with both static and dynamic structures.

This paper is outlined as follows; In Section II, we formulate the dynamic model of our fully actuated aerial manipulator, and the control framework that includes DOB-based control law and safety filter is introduced in Section III. In Section IV, we present a theoretical analysis on the safety filter, and Section V covers the experimental validation of the proposed method.

Notations: $\mathbf{0}_{i \times j}$, \mathbf{I}_i , \mathbf{e}_3 and $\mathbf{E}_i \in \mathbb{R}^6$ represent the $i \times j$ zero matrix, $i \times i$ identity matrix, $[0; 0; 1]$ and \mathbb{R}^6 vector where its i^{th} element is one and the other elements are zero, respectively. For scalars a_1, \dots, a_N , we let $c a_1$ and $s a_1$ denote $\cos a_1$ and $\sin a_1$, respectively, and $\text{diag}\{a_1, \dots, a_N\}$ represents an $N \times N$ diagonal matrix where the $(i, i)^{\text{th}}$ element is a_i and all off-diagonal elements are zero. For vectors α and β , we let α_i denote the i -th element of α , and if $\alpha \in \mathbb{R}^3$ and $\beta \in \mathbb{R}^3$, $[\alpha]_{\times} \in \mathbb{R}^{3 \times 3}$ means the operator which maps α into a skew-symmetric matrix such as $[\alpha]_{\times} \beta = \alpha \times \beta$. Also, for matrices $\mathbf{A}_1, \dots, \mathbf{A}_N$, $\text{blkdiag}\{\mathbf{A}_1, \dots, \mathbf{A}_N\}$ represents a block diagonal matrix obtained by aligning $\mathbf{A}_1, \dots, \mathbf{A}_N$. Moreover, we abbreviate the phrase "with respect to" to w.r.t..

II. MODELLING

Fig. 2 illustrates an aerial manipulator configured with a fully actuated multirotor with six tilted motors and a rigidly

attached robotic arm. Also, two key coordinate frames, the Earth-fixed frame \mathcal{F}_W and the multirotor frame \mathcal{F}_b , are displayed.

The generalized coordinate of the aerial manipulator, $\mathbf{q} \triangleq [\mathbf{p}; \phi]$, consists of the position of \mathcal{F}_b w.r.t. \mathcal{F}_W expressed in \mathcal{F}_W , $\mathbf{p} \in \mathbb{R}^3$, and ZYX Euler angles, $\phi \in \mathbb{R}^3$. Then, the Euler-Lagrange model of the aerial manipulator is formulated as follows [14]:

$$\mathbf{M}(\phi)\ddot{\mathbf{q}} + \mathbf{C}(\phi, \dot{\phi}) + \mathbf{G} = \boldsymbol{\tau} + \boldsymbol{\tau}_{ext} \quad (1)$$

where $\boldsymbol{\tau} \in \mathbb{R}^6$ and $\boldsymbol{\tau}_{ext} \in \mathbb{R}^6$ represent the generalized control wrench and external disturbance, respectively, and

$$\mathbf{M}(\phi) \triangleq \begin{bmatrix} m\mathbf{I}_3 & \mathbf{0}_{3 \times 3} \\ \mathbf{0}_{3 \times 3} & \mathbf{Q}^T \mathbf{J} \mathbf{Q} \end{bmatrix},$$

$$\mathbf{C}(\phi, \dot{\phi}) \triangleq \begin{bmatrix} \mathbf{0}_{3 \times 1} \\ \mathbf{Q}^T (\mathbf{J} \dot{\mathbf{Q}} \dot{\phi} + [\mathbf{Q} \dot{\phi}]_{\times} \mathbf{J} \mathbf{Q} \dot{\phi}) \end{bmatrix}, \quad \mathbf{G} \triangleq \begin{bmatrix} m g \mathbf{e}_3 \\ \mathbf{0}_{3 \times 1} \end{bmatrix}$$

with the mass and moment of inertia of the aerial manipulator, m and $\mathbf{J} \in \mathbb{R}^{3 \times 3}$, and the gravitational acceleration, g . Also, we let $\mathbf{Q} \in \mathbb{R}^{3 \times 3}$ denote the mapping matrix satisfying $\boldsymbol{\omega} = \mathbf{Q} \dot{\phi}$ where $\boldsymbol{\omega} \in \mathbb{R}^3$ represents the angular velocity of the vehicle w.r.t. \mathcal{F}_W expressed in \mathcal{F}_b . Meanwhile, the relationship between $\boldsymbol{\tau}$ and $\mathbf{T} \triangleq [T_1; \dots; T_6]$ is derived as follows:

$$\boldsymbol{\tau} = \mathbf{B}(\phi) \boldsymbol{\Xi} \mathbf{T} \quad (2)$$

where $\mathbf{B}(\phi) \triangleq \text{blkdiag}\{\mathbf{R}, \mathbf{Q}^T\}$ and

$$\boldsymbol{\Xi} \triangleq \begin{bmatrix} \frac{1}{2} s \alpha & -s \alpha & \frac{1}{2} s \alpha & \frac{1}{2} s \alpha & -s \alpha & \frac{1}{2} s \alpha \\ -\frac{\sqrt{3}}{2} s \alpha & 0 & \frac{\sqrt{3}}{2} s \alpha & -\frac{\sqrt{3}}{2} s \alpha & 0 & \frac{\sqrt{3}}{2} s \alpha \\ c \alpha & c \alpha & c \alpha & c \alpha & c \alpha & c \alpha \\ -\frac{1}{2} P_1 & -P_1 & -\frac{1}{2} P_1 & \frac{1}{2} P_1 & P_1 & \frac{1}{2} P_1 \\ \frac{\sqrt{3}}{2} P_1 & 0 & -\frac{\sqrt{3}}{2} P_1 & -\frac{\sqrt{3}}{2} P_1 & 0 & \frac{\sqrt{3}}{2} P_1 \\ P_2 & -P_2 & P_2 & -P_2 & P_2 & -P_2 \end{bmatrix}. \quad (3)$$

with $P_1 \triangleq L c \alpha + k_f s \alpha$ and $P_2 \triangleq L s \alpha - k_f c \alpha$. In (3), L , α and k_f represent the length from the vehicle's origin to each propeller, fixed tilt angle of each motor and thrust-to-torque coefficient, respectively.

To address the effect of model uncertainties, we rearrange (1) as follows:

$$\hat{\mathbf{M}}(\phi)\ddot{\mathbf{q}} + \hat{\mathbf{C}}(\phi, \dot{\phi}) + \hat{\mathbf{G}} = \boldsymbol{\tau} + \mathbf{d} \quad (4)$$

where $\hat{\mathbf{M}}(\phi)$, $\hat{\mathbf{C}}(\phi, \dot{\phi})$ and $\hat{\mathbf{G}}$ are the nominal values of $\mathbf{M}(\phi)$, $\mathbf{C}(\phi, \dot{\phi})$ and \mathbf{G} , respectively, and the lumped disturbance $\mathbf{d} \in \mathbb{R}^6$ satisfies:

$$\mathbf{d} \triangleq (\hat{\mathbf{M}}(\phi) - \mathbf{M}(\phi))\ddot{\mathbf{q}} + \hat{\mathbf{C}}(\phi, \dot{\phi}) - \mathbf{C}(\phi, \dot{\phi}) + \hat{\mathbf{G}} - \mathbf{G} + \boldsymbol{\tau}_{ext}.$$

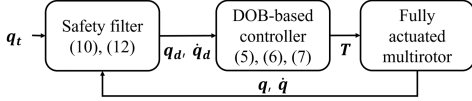


Fig. 3. Overall controller diagram for safe APhI

III. CONTROL FRAMEWORK

A DOB-based controller introduced in [15] makes the state of a robotic system follow its desired trajectory within a small bound for all $t \geq t_0$ even under the effect of time-varying external disturbances and model uncertainties. Hence, we adopt this control structure to conduct APhI. However, if it is not dynamically feasible to reach the vehicle's target pose, e.g., the target position is inside the wall while exerting on a static wall, the aerial system may become unstable since one of the motors cannot generate the commanded thrust value due to its limit. Thus, we need a safety filter that modifies the desired pose trajectory based on the system model (4), the DOB's structure and the feasible range of the motor thrust.

Fig. 3 presents the overall controller diagram for safe APhI. Based on the target pose set by an external planner (e.g., joystick or ground computer station), $\mathbf{q}_t \in \mathbb{R}^6$, the desired pose and twist, $\mathbf{q}_d \in \mathbb{R}^6$ and $\dot{\mathbf{q}}_d \in \mathbb{R}^6$, are calculated by the safety filter. Then, the DOB-based control law generates \mathbf{T} .

A. DOB-Based Control Law

According to [15], the estimation of the lumped disturbance, $\hat{\mathbf{d}} \in \mathbb{R}^6$, is formulated as follows:

$$\begin{aligned} \hat{\mathbf{d}} &= -\hat{\mathbf{M}}(\phi)(\mu^{-1}\Gamma_\zeta(\zeta - \dot{\mathbf{q}}) + \chi) + \hat{\mathbf{C}}(\phi, \dot{\phi}) + \hat{\mathbf{G}} \\ \dot{\zeta} &= -\mu^{-1}\Gamma_\zeta(\zeta - \dot{\mathbf{q}}) \\ \dot{\chi} &= -\mu^{-1}\Gamma_\chi(\chi - \hat{\mathbf{M}}^{-1}(\phi)\tau) \end{aligned} \quad (5)$$

where $\zeta \in \mathbb{R}^6$ and $\chi \in \mathbb{R}^6$ represent the filtered values of $\dot{\mathbf{q}}$ and $\hat{\mathbf{M}}^{-1}(\phi)\tau$, respectively, with constant positive definite matrices $\Gamma_\zeta, \Gamma_\chi \in \mathbb{R}_{>0}^{6 \times 6}$ and a matrix $\mu \triangleq \text{diag}\{\mu_1, \dots, \mu_6\}$ configured with positive constants lower than one. Then, based on \mathbf{q}_d and $\dot{\mathbf{q}}_d$ acquired from the safety filter, the control law for τ is designed as follows:

$$\tau(\mathbf{x}) = \hat{\mathbf{M}}(\phi)(\mathbf{K}_d \dot{\mathbf{e}} + \mathbf{K}_p \mathbf{e}) + \hat{\mathbf{C}}(\phi, \dot{\phi}) + \hat{\mathbf{G}} - \hat{\mathbf{d}} \quad (6)$$

where $\mathbf{e} \triangleq \mathbf{q}_d - \mathbf{q}$ and $\mathbf{x} \triangleq [\mathbf{q}; \dot{\mathbf{q}}; \zeta; \chi; \mathbf{q}_d; \dot{\mathbf{q}}_d]$ with controller gains $\mathbf{K}_p \in \mathbb{R}_{>0}^{6 \times 6}$ and $\mathbf{K}_d \in \mathbb{R}_{>0}^{6 \times 6}$. By (2), $\mathbf{T}(\mathbf{x})$ is calculated as follows:

$$\mathbf{T}(\mathbf{x}) = \Xi^{-1} \mathbf{B}^{-1}(\phi) \tau(\mathbf{x}). \quad (7)$$

B. Safety Filter

In the safety filter, \mathbf{q}_d and $\dot{\mathbf{q}}_d$ is adjusted based on (4) - (6) and the limit of motor thrust. To this end, we need to formulate a control-affine system with \mathbf{x} as a state and the vehicle's acceleration $\ddot{\mathbf{q}}_d \in \mathbb{R}^6$ as an input.

By substituting (5) and (6) for (4), we obtain the system w.r.t. \mathbf{x} as follows:

$$\dot{\mathbf{x}} = \mathbf{f}(\mathbf{x}) + \mathbf{g}\ddot{\mathbf{q}}_d + \rho(\mathbf{x}, \tilde{\mathbf{d}}) \quad (8)$$

where $\mathbf{g} = [\mathbf{0}_{30 \times 6}; \mathbf{I}_6]$, $\rho(\mathbf{x}, \tilde{\mathbf{d}}) = [\mathbf{0}_{6 \times 1}; -\hat{\mathbf{M}}^{-1}(\phi)\tilde{\mathbf{d}}; \mathbf{0}_{24 \times 1}]$ and

$$\mathbf{f}(\mathbf{x}) = \begin{bmatrix} \dot{\mathbf{q}} \\ \mathbf{K}_d \dot{\mathbf{e}} + \mathbf{K}_p \mathbf{e} \\ -\mu^{-1}\Gamma_\zeta(\zeta - \dot{\mathbf{q}}) \\ \mu^{-1}\Gamma_\chi(\mathbf{K}_d \dot{\mathbf{e}} + \mathbf{K}_p \mathbf{e} + \mu^{-1}\Gamma_\zeta(\zeta - \dot{\mathbf{q}})) \\ \dot{\mathbf{q}}_d \\ \mathbf{0}_{6 \times 1} \end{bmatrix}.$$

Our main objective is to make \mathbf{x} stay inside its safety set constructed as:

$$\mathcal{C}_T \triangleq \{\mathbf{x} \in \mathbb{R}^{36} \mid T_m \leq T_i(\mathbf{x}) \leq T_M, i = 1, \dots, 6\}$$

where T_m and T_M are the minimum and maximum values of each motor's thrust. Hence, we first define six barrier functions $h_{T,1}(\mathbf{x}), \dots, h_{T,6}(\mathbf{x})$ as follows:

$$h_{T,i}(\mathbf{x}) \triangleq \left(\frac{T_M - T_m}{2}\right)^2 - (T_i(\mathbf{x}) - \frac{T_M + T_m}{2})^2 \quad (9)$$

so that $\mathcal{C}_T = \mathcal{C}_{T,1} \cap \dots \cap \mathcal{C}_{T,6}$ with $\mathcal{C}_{T,i} \triangleq \{\mathbf{x} \in \mathbb{R}^{36} \mid h_{T,i}(\mathbf{x}) \geq 0\}$. To ensure that $T_i(\mathbf{x})$ does not violate its limit for all $t \geq t_0$, the desired acceleration of the vehicle, $\ddot{\mathbf{q}}_d$, has to satisfy the following inequality:

$$0 \leq \dot{h}_{T,i}(\mathbf{x}, \dot{\mathbf{x}}) + \gamma_{T,i} h_{T,i}(\mathbf{x}), \forall (x, i) \in \mathcal{D} \times \{1, \dots, 6\}$$

where $\gamma_{T,i}$ is a user-defined constant parameter and $\mathcal{D} \subset \mathbb{R}^{36}$ means the domain of \mathbf{x} .

1) *Compensation for DOB Error:* According to (8), $\dot{h}_{T,i}(\mathbf{x}, \dot{\mathbf{x}})$ is calculated as $\mathcal{L}_f h_{T,i}(\mathbf{x}) + \mathcal{L}_g h_{T,i}(\mathbf{x}) \ddot{\mathbf{q}}_d + \frac{\partial h_{T,i}(\mathbf{x})}{\partial \mathbf{x}} \rho(\mathbf{x}, \tilde{\mathbf{d}})$ and consists of an unknown term $\beta_{T,i}(\mathbf{x}, \tilde{\mathbf{d}}) \triangleq \frac{\partial h_{T,i}(\mathbf{x})}{\partial \mathbf{x}} \rho(\mathbf{x}, \tilde{\mathbf{d}})$. Therefore, we estimate this term by utilizing the method introduced in [16] as follows:

$$\begin{aligned} \hat{\beta}_{T,i}(\mathbf{x}, \xi_{T,i}) &= k_{\beta,T,i} h_{T,i}(\mathbf{x}) - \xi_{T,i} \\ \dot{\xi}_{T,i} &= k_{\beta,T,i} \{\mathcal{L}_f h_{T,i}(\mathbf{x}) + \mathcal{L}_g h_{T,i}(\mathbf{x}) \ddot{\mathbf{q}}_d + \hat{\beta}_{T,i}(\mathbf{x}, \xi_{T,i})\} \end{aligned} \quad (10)$$

with a positive constant parameter $k_{\beta,T,i} > \gamma_{T,i}$. According to [16], (10) guarantees the following inequality:

$$|e_{T,i}(t)| \leq (|e_{T,i}(t_0)| - \frac{\beta_{T,h,i}}{k_{\beta,T,i}}) e^{-k_{\beta,T,i}(t-t_0)} + \frac{\beta_{T,h,i}}{k_{\beta,T,i}} \quad (11)$$

where $e_{T,i} \triangleq \beta_{T,i}(\mathbf{x}, \tilde{\mathbf{d}}) - \hat{\beta}_{T,i}(\mathbf{x}, \xi_{T,i})$ and $\beta_{T,h,i} \geq |\frac{d}{dt} \beta_{T,i}(\mathbf{x}, \tilde{\mathbf{d}})|$

2) *Quadratic Programming (QP) Problem on Solving Desired Acceleration:* Since there exists a difference between $\beta_{T,i}(\mathbf{x}, \tilde{\mathbf{d}})$ and $\hat{\beta}_{T,i}(\mathbf{x}, \xi_{T,i})$, we define a more conservative inequality on $\ddot{\mathbf{q}}_d$ as follows:

$$\begin{aligned} \sigma_{T,i} \leq & \mathcal{L}_f h_{T,i}(\mathbf{x}) + \mathcal{L}_g h_{T,i}(\mathbf{x}) \ddot{\mathbf{q}}_d \\ & + \hat{\beta}_{T,i}(\mathbf{x}, \xi_{T,i}) + \gamma_{T,i} h_{T,i}(\mathbf{x}) \end{aligned}$$

with the positive scalars $\sigma_{T,1}, \dots, \sigma_{T,6}$. According to [16], if $\sigma_{T,i} \geq \max\{|e_{T,i}(t_0)|, \frac{\beta_{T,h,i}}{k_{\beta,T,i}}\}$, then $0 \leq \dot{h}_{T,i}(\mathbf{x}, \dot{\mathbf{x}}) + \gamma_{T,i} h_{T,i}(\mathbf{x})$. Also, since the boundedness of $\tilde{\mathbf{d}}$ and

$\dot{\tilde{\mathbf{d}}}$ is proven in [15] and $|e_{T,i}(t_0)|$ is also bounded, we can find a large number $\sigma_{T,i}$ such that $\sigma_{T,i} \geq \max\{|e_{T,i}(t_0)|, \frac{\beta_{T,h,i}}{k_{\beta,T,i}}\}$, $\forall i \in \{1, \dots, 6\}$.

Accordingly, the quadratic programming (QP) problem with the decision variable $\tilde{\mathbf{q}}_d$ is formulated as follows:

$$\min_{\tilde{\mathbf{q}}_d} \|\tilde{\mathbf{q}}_d - \tilde{\mathbf{q}}_t\|^2 \text{ s.t. } \mathbf{A}_T \tilde{\mathbf{q}}_d + \boldsymbol{\sigma}_T \leq \hat{\mathbf{b}}_T \quad (12)$$

where $\mathbf{A}_T \triangleq -[\mathcal{L}_g h_{T,1}(\mathbf{x}); \mathcal{L}_g h_{T,2}(\mathbf{x}); \dots; \mathcal{L}_g h_{T,6}(\mathbf{x})]$, $\boldsymbol{\sigma}_T \triangleq [\sigma_{T,1}; \dots; \sigma_{T,6}]$ and

$$\hat{\mathbf{b}}_T \triangleq \begin{bmatrix} \gamma_{T,1}(h(\mathbf{x})) + \mathcal{L}_f h_{T,1}(\mathbf{x}) + \hat{\beta}_{T,1}(\mathbf{x}, \xi_{T,1}) \\ \vdots \\ \gamma_{T,6}(h(\mathbf{x})) + \mathcal{L}_f h_{T,6}(\mathbf{x}) + \hat{\beta}_{T,6}(\mathbf{x}, \xi_{T,6}) \end{bmatrix}.$$

The target acceleration $\tilde{\mathbf{q}}_t \in \mathbb{R}^6$ will be presented in the next section, and the detailed expression of Lie derivatives $\mathcal{L}_f h_{T,i}(\mathbf{x})$ and $\mathcal{L}_g h_{T,i}(\mathbf{x})$ can be found in Appendix.

3) *Target Acceleration Calculation:* The target acceleration, $\tilde{\mathbf{q}}_t \in \mathbb{R}^6$, is calculated as follows:

$$\ddot{q}_{t,i} = -2k_{a,i}\delta_{v,i}\dot{q}_{d,i} - k_{a,i}^2(q_{t,i} - q_{d,i}), \quad i = 1, \dots, 6 \quad (13)$$

where $k_{a,i}$ is a positive scalar and

$$\delta_{v,i} = \delta_{v,m} + \frac{k_{\Delta p}|q_{d,i} - q_{t,i}|}{1 + k_{\Delta p}|q_{d,i} - q_{t,i}|}(\delta_{v,M} - \delta_{v,m}) \quad (14)$$

with the minimum and maximum damping ratios, $\delta_{v,m}$ and $\delta_{v,M}$, and the proportional gain to the target-desired pose difference, $k_{\Delta p}$. (14) indicates that the magnitude of the desired twist can be reduced by increasing the damping ratio if the difference between the desired and target poses gets larger. It prevents excessive oscillation of \mathbf{q}_d and $\dot{\mathbf{q}}_d$.

IV. THEORETICAL ANALYSIS

Theorem 1: Let $\mathbf{h}_T(\mathbf{x})$ denote $[h_{T,1}(\mathbf{x}); \dots; h_{T,6}(\mathbf{x})]$, then the safety set \mathcal{C}_T is forward invariant with (4), (5), (6), (10) and (12).

Proof: From (12), the inequality $\mathbf{A}_T \tilde{\mathbf{q}}_d + \boldsymbol{\sigma}_T \leq \hat{\mathbf{b}}_T$ is rearranged as $\mathbf{A}_T \tilde{\mathbf{q}}_d \leq \mathbf{b}_T - \mathbf{e}_T - \boldsymbol{\sigma}_T$ where $\mathbf{e}_T \triangleq [e_{T,1}; \dots; e_{T,6}]$ and

$$\mathbf{b}_T \triangleq \begin{bmatrix} \gamma_{T,1}(h(\mathbf{x})) + \mathcal{L}_f h_{T,1}(\mathbf{x}) + \beta_{T,1}(\mathbf{x}, \tilde{\mathbf{d}}) \\ \vdots \\ \gamma_{T,6}(h(\mathbf{x})) + \mathcal{L}_f h_{T,6}(\mathbf{x}) + \beta_{T,6}(\mathbf{x}, \tilde{\mathbf{d}}) \end{bmatrix}.$$

Since $\mathbf{b}_T - \mathbf{A}_T \tilde{\mathbf{q}}_d = \dot{\mathbf{h}}_T(\mathbf{x}, \dot{\mathbf{x}}) + \boldsymbol{\Gamma}_T \mathbf{h}_T(\mathbf{x})$ where $\boldsymbol{\Gamma}_T \triangleq \text{diag}\{\gamma_{T,1}; \dots; \gamma_{T,6}\}$, $\mathbf{A}_T \tilde{\mathbf{q}}_d \leq \mathbf{b}_T - \mathbf{e}_T - \boldsymbol{\sigma}_T$ is reformulated as $\mathbf{e}_T + \boldsymbol{\sigma}_T \leq \dot{\mathbf{h}}_T(\mathbf{x}, \dot{\mathbf{x}}) + \boldsymbol{\Gamma}_T \mathbf{h}_T$. Because $-|e_{T,i}| \leq e_{T,i} \leq |e_{T,i}|$, (11) is arranged as $e_{T,i}(t) \geq (\frac{\beta_{T,h,i}}{k_{\beta,T,i}} - |e_{T,i}(t_0)|)e^{-k_{\beta,T,i}(t-t_0)} - \frac{\beta_{T,h,i}}{k_{\beta,T,i}}$. Then, from the proof of [16, Theorem 1], we obtain $e_{T,i}(t) + \sigma_{T,i} \geq (\max\{|e_{T,i}(t_0)|, \frac{\beta_{T,h,i}}{k_{\beta,T,i}}\} - |e_{T,i}(t_0)|)e^{-k_{\beta,T,i}(t-t_0)} + \sigma_{T,i} - \max\{|e_{T,i}(t_0)|, \frac{\beta_{T,h,i}}{k_{\beta,T,i}}\}$. Since $\sigma_{T,i} \geq \max\{|e_{T,i}(t_0)|, \frac{\beta_{T,h,i}}{k_{\beta,T,i}}\}$, we prove that $e_{T,i}(t) +$

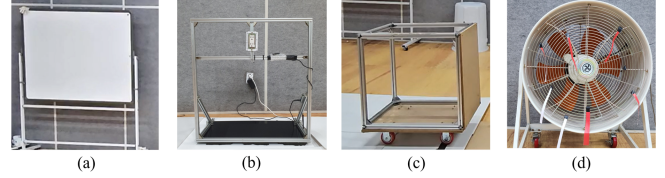


Fig. 4. Equipment utilized in the actual experiments: (a) a vertical whiteboard, (b) a frame with a 110 V electric socket, (c) a wheeled cart, and (d) an industrial fan.

$\sigma_{T,i} \geq 0$. Therefore, the following statement is true for all $\mathbf{x} \in \mathcal{D}$ and for all $t > t_0$:

$$\mathbf{A}_T \tilde{\mathbf{q}}_d + \boldsymbol{\sigma}_T \leq \hat{\mathbf{b}}_T \rightarrow \mathbf{0}_{6 \times 1} \leq \dot{\mathbf{h}}_T(\mathbf{x}, \dot{\mathbf{x}}) + \boldsymbol{\Gamma}_T \mathbf{h}_T. \quad (15)$$

According to Appendix, $\mathcal{L}_g h_{T,i}(\mathbf{x})$ is $-2(T_i(\mathbf{x}) - \frac{T_M + T_m}{2})\mathbf{E}_i^\top \mathbf{J}_a(\phi)\mathbf{K}_d$ where $\mathbf{J}_a(\phi) = \boldsymbol{\Xi}^{-1}\mathbf{B}^{-1}(\phi)\hat{\mathbf{M}}(\phi)$. Thus, \mathbf{A}_T in (12) is calculated as $-2\text{diag}\{[T_1(\mathbf{x}) - \frac{T_M + T_m}{2}; \dots; T_6(\mathbf{x}) - \frac{T_M + T_m}{2}]\}\mathbf{J}_a(\phi)\mathbf{K}_d$. Since $\boldsymbol{\Xi}$, $\mathbf{B}(\phi)$, $\hat{\mathbf{M}}(\phi)$ and \mathbf{K}_d are all invertible matrices for all $\phi \in [-\pi, \pi] \times (-\frac{\pi}{2}, \frac{\pi}{2}) \times [-\pi, \pi]$, $\mathbf{J}_a(\phi)\mathbf{K}_d$ is also invertible.

Let $\mathcal{N}_{T=0} \subset \{1, \dots, 6\}$ denote the set of indices that $T_i = \frac{T_M + T_m}{2}$, then we can analyze $\mathbf{A}_T \tilde{\mathbf{q}}_d + \boldsymbol{\sigma}_T \leq \hat{\mathbf{b}}_T$ row-by-row as follows:

- If $i \in \mathcal{N}_{T=0}$, then $\frac{\partial h_{T,i}}{\partial \mathbf{x}}$ becomes $\mathbf{0}_{1 \times 36}$ since $\frac{\partial h_{T,i}}{\partial \mathbf{x}} = -2(T_i(\mathbf{x}) - \frac{T_M + T_m}{2})\mathbf{E}_i^\top \frac{\partial T}{\partial \mathbf{x}}$. Thus, $\dot{h}_{T,i}(\mathbf{x}, \dot{\mathbf{x}})$ becomes zero so that $0 \leq \dot{h}_{T,i}(\mathbf{x}, \dot{\mathbf{x}}) + \gamma_{T,i}h_{T,i}(\mathbf{x})$ holds.
- Let $i_{f,1}, \dots, i_{f,n_T}$ denote the elements of $\mathcal{N}_{T \neq 0} \triangleq \{1, \dots, 6\} - \mathcal{N}_{T=0}$ where n_T represents the number of elements in $\mathcal{N}_{T \neq 0}$, then the inequality $\mathbf{A}_T \tilde{\mathbf{q}}_d + \boldsymbol{\sigma}_T \leq \hat{\mathbf{b}}_T$ is rearranged as follows:

$$\mathbf{A}_{T, \mathcal{N}_{T \neq 0}} \tilde{\mathbf{q}}_d \leq \mathbf{b}_{T, \mathcal{N}_{T \neq 0}} \quad (16)$$

where

$$\mathbf{A}_{T, \mathcal{N}_{T \neq 0}} \triangleq -2 \begin{bmatrix} (T_{i_{f,1}}(\mathbf{x}) - \frac{T_m + T_M}{2})\mathbf{E}_{i_{f,1}}^\top \\ \vdots \\ (T_{i_{f,n_T}}(\mathbf{x}) - \frac{T_m + T_M}{2})\mathbf{E}_{i_{f,n_T}}^\top \end{bmatrix} \times \mathbf{J}_a(\phi)\mathbf{K}_d$$

$$\mathbf{b}_{T, \mathcal{N}_{T \neq 0}} \triangleq [b_{T,i_{f,1}} - \sigma_{T,i_{f,1}}; \dots; b_{T,i_{f,n_T}} - \sigma_{T,i_{f,n_T}}].$$

Since $\mathbf{J}_a(\phi)\mathbf{K}_d$ is invertible, the rank of $\mathbf{A}_{T, \mathcal{N}_{T \neq 0}}$ is N_T unless $N_T = 0$. Thus, there exists $\tilde{\mathbf{q}}_d^* \in \mathbb{R}^6$ such that $\mathbf{A}_{T, \mathcal{N}_{T \neq 0}} \tilde{\mathbf{q}}_d^* = \mathbf{b}_{T, \mathcal{N}_{T \neq 0}} - \mathbf{b}_{T,r}$ where all the elements of $\mathbf{b}_{T,r} \in \mathbb{R}^{N_T}$ are positive scalars.

From the above discussion, we prove that there exists $\tilde{\mathbf{q}}_{d,sol} \in \mathbb{R}^6$ satisfying $\mathbf{A}_T \tilde{\mathbf{q}}_{d,sol} + \boldsymbol{\sigma}_T \leq \hat{\mathbf{b}}_T$ for all $(\mathbf{x}, t) \in \mathcal{D} \times [t_0, \infty)$. Hence, from (15), we prove that $\mathbf{0}_{6 \times 1} \leq \dot{\mathbf{h}}_T(\mathbf{x}, \dot{\mathbf{x}}) + \boldsymbol{\Gamma}_T \mathbf{h}_T$ holds so that \mathcal{C}_T is rendered forward invariance with (4), (5), (6), (10) and (12). ■

V. EXPERIMENTAL RESULTS

To validate the performance of the proposed controller in various types of APH, we conduct actual experiments with the following four scenarios:

- 1) Pushing a static whiteboard (Fig. 1(a)).
- 2) Pulling a firmly attached plug (Fig. 1(b)).
- 3) Pushing a movable cart (Fig. 1(c)).
- 4) Pulling a plug out of a 110 V electric socket (Fig. 1(b)).

For scenarios 1) and 2), we compare the results from the proposed controller with two other existing controllers to show the enhanced control performance. For scenarios 3) and 4), we conduct repetitive experiments with the proposed controller to validate that our controller can repeatedly perform tasks involving sudden changes in dynamics.

A. Experimental Setups

The aerial manipulator utilized for this work consists of two parts: a fully actuated hexacopter and a rigidly attached robotics arm. The fully actuated hexacopter which weighs 3.50 kg was assembled with the off-the-shelf frame DJI F550, six 9-inch APC LPB09045MR propellers, six KDE2314XF-965 motors with corresponding KDEXF-UAS35 electronic speed controllers (ESCs), six 3D printed thrust-tilting frames with $\alpha = 15^\circ$, a 4S Turnigy Lipo battery to power up Intel NUC, a 6S Polytronics Lipo battery for the power supplement of the six ESCs, and Intel NUC for computing. On Intel NUC, Robot Operating System (ROS) noetic version is installed in Ubuntu 20.04, and the proposed control algorithm for the hexacopter and the navigation algorithm with Optitrack are executed. In the customized Pixhawk 4 connected to the Intel NUC, the rotational speeds of the six motors are controlled.

For all the experiments, an industrial fan shown in Fig. 4(d) is used to generate a wind blast to imitate a more realistic situation, the parameter values are set as shown in Table I, and the target pose q_t is set from the human operator's laptop.

TABLE I
PARAMETER VALUES UTILIZED IN EXPERIMENTS.

\hat{m}	3.50	T_m	1.0
\hat{g}	9.81	T_M	15
\hat{J}	diag{[0.035;0.035;0.045]}	$\gamma_{T,i=1,\dots,6}$	10
K_p	diag{[6.0,6.0,8.0,70,70,55]}	$k_{\beta,T,i=1,\dots,6}$	10.1
K_d	diag{[4.0,4.0,5.0,30,30,15]}	$\sigma_{T,i=1,\dots,6}$	15
Γ_ζ	diag{[1.0,1.0,1.0,0.10,0.10,0.50]}	$k_{a,i=1,2,3,6}$	1.0
Γ_χ	diag{[1.0,1.0,1.0,0.10,0.10,0.50]}	$k_{a,i=1,2,3,6}$	5.0
$\mu_{i=4,5}$	0.80	$\mu_{i=1,2,3,6}$	0.95

B. Controller Comparison: Scenarios 1) and 2)

For the scenarios 1) and 2), we compare the performance of the proposed method with two other baselines shown below:

- First baseline: Without a safety filter.
- Second baseline: Direct adjustment of τ based on τ_t calculated as in (6) instead of adjusting q_d and \dot{q}_d .
- Proposed: The proposed safety filter.

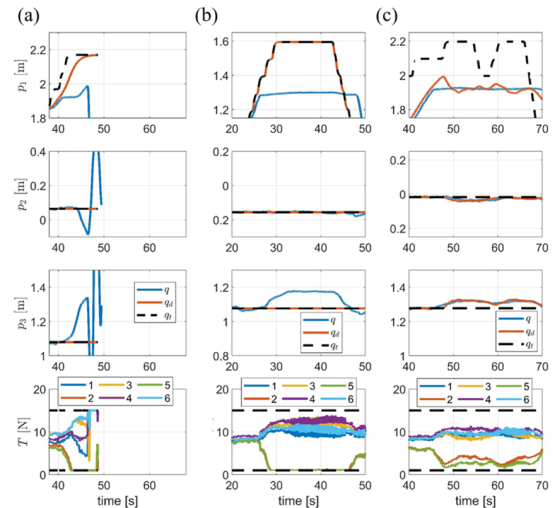


Fig. 5. Histories of the vehicle's position (p) and motor thrust values (T_1, \dots, T_6) during the static whiteboard-pushing experiment with (a) the first baseline, (b) second baseline, and (c) the proposed method.

1) *Pushing a Static Whiteboard*: For this scenario, we set $k_{\delta p}$, $\delta_{v,m}$ and $\delta_{v,M}$ as 0.5, 1.0 and 5.0, respectively. The human operator manually commanded the aerial manipulator to reach 0.3 m beyond the location of the whiteboard to exert pushing force on its surface.

Fig. 5 presents the histories of the target, desired and actual position, and those of each motor's thrust. As observed in Fig. 5(a), the vehicle failed to maintain its stability without any safety filter. Otherwise, in Figs. 5(b) and 5(c), we can notice that the vehicle successfully maintains its stability while pushing the whiteboard with the second baseline and proposed method. Even though there is no big difference between the results with the second baseline and the proposed method, we can note that p_3 shows slightly less overshoot with the proposed method.

2) *Pulling a Firmly Attached Plug*: For this scenario, we set $k_{\delta p}$, $\delta_{v,m}$ and $\delta_{v,M}$ as 5.0, 1.0, and 5.0, respectively. To make a pulling movement, the operator set the target pose to 0.2 m away from the socket.

Likewise in Fig. 5(a), from Fig. 6(a), we can observe that the aerial manipulator showed an oscillating behavior without any safety filter while pulling the plug firmly attached to the socket. On the other hand, Figs. 6(b) and 6(c) indicate that the second baseline and the proposed method lead to the vehicle's safe pulling. However, from the plot of T in Fig. 6(b), we can note that there occurred a large oscillation in motor thrust. In the attached video, we can observe the large oscillation of roll and pitch angles due to the oscillating behavior of the motor thrust.

C. Validation on Tasks Involving Sudden Changes in Dynamics: : Scenarios 3) and 4)

Through scenarios 3) and 4), we aim to emphasize the proposed method's repeatability in situations involving sudden changes in dynamics such as the sudden disappearance of the interaction wrench. Hence, we conducted five repetitive experiments for each task.

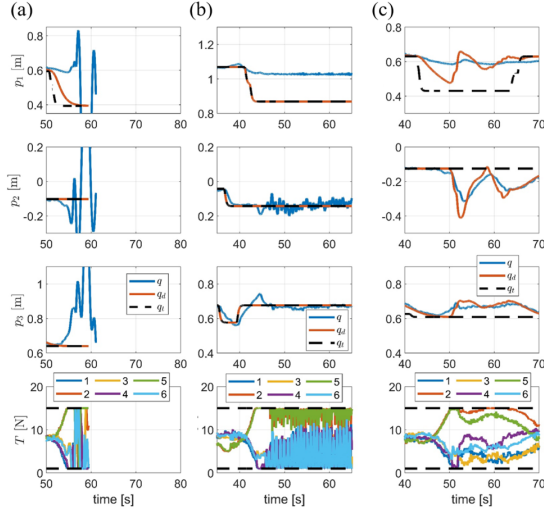


Fig. 6. Histories of the vehicle's position (\mathbf{p}) and motor thrust values (T_1, \dots, T_6) while pulling a firmly attached plug with (a) the first baseline, (b) second baseline, and (c) the proposed method.

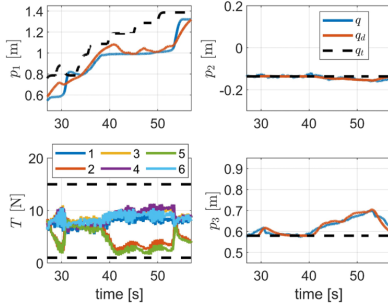


Fig. 7. Histories of the vehicle's position (\mathbf{p}) and motor thrust values (T_1, \dots, T_6) of the first cart-pushing experiment.

1) *Pushing a Movable Cart*: For this scenario, $k_{\delta p}$, $\delta_{v,m}$ and $\delta_{v,M}$ are set as 0.5, 1.0, and 5.0, respectively. We commanded the aerial manipulator to consistently push the cart (Fig. 4(c)) until its rear wheels go over the left black line shown in Fig. 1(c).

Fig. 7 reports the histories of the vehicle's position and motor thrust while conducting the first one among five cart-pushing experiments. As seen in the position plots, p_d actively modifies its value accordingly with the cart's movement.

2) *Pulling a Plug out of the Socket*: For this scenario, we put 5.0, 1.0, and 5.0 into $k_{\delta p}$, $\delta_{v,m}$ and $\delta_{v,M}$, respectively, and set $p_{t,1} = q_{t,1}$ as 0.2 m away from the grabbing position.

In Fig. 8, the position and thrust histories of the fourth one among five plug-pulling experiments. In the left upper plot of Fig. 8, the history of q_1 shows that the plug is extracted around 57 seconds and the vehicle successfully stabilizes right after the plug separation.

VI. CONCLUSIONS

This paper presented a safety filter based on a disturbance observer (DOB)-based control structure, designed to enhance pose-tracking performance while ensuring flight safety during physical interaction. First, we derived the Lagrange-Euler

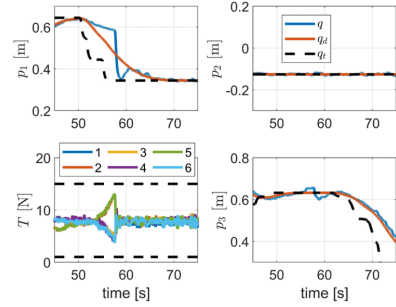


Fig. 8. Histories of the vehicle's position (\mathbf{p}) and motor thrust values (T_1, \dots, T_6) of the fourth plug-pulling experiment.

model for an aerial manipulator consisting of a fully actuated hexacopter and a rigidly attached robotic arm. Using this model, we developed a safety filter that accounted for motor thrust limits, external disturbances, and model uncertainties, integrated with the DOB-based control method. We also proved that the proposed safety filter and controller ensured forward invariance of the safety set with respect to motor thrust limits. To validate the performance of the proposed method over existing control strategies for aerial physical interaction (APHI), we conducted comparative experiments. These included pushing a static structure and pulling a firmly attached object using the aerial manipulator. Additionally, we performed repeated tests on tasks with sudden dynamic changes, such as pushing a movable cart and extracting a plug from a socket, to verify the controller's ability to handle these dynamic shifts. Future work may involve designing a hybrid controller to better manage abrupt changes in dynamic models or extending the system for haptic-based teleoperation of an aerial manipulator interacting with its environment.

APPENDIX

The detailed expressions of the Lie derivatives are calculated as follows:

$$\begin{aligned} \mathcal{L}_f h_{T,i}(\mathbf{x}) &= -2(T_i(\mathbf{x}) - \frac{T_m + T_M}{2}) \mathbf{E}_i^\top \frac{\partial T}{\partial \mathbf{x}}(\mathbf{x}) \mathbf{f}(\mathbf{x}), \\ \mathcal{L}_g h_{T,i}(\mathbf{x}) &= -2(T_i(\mathbf{x}) - \frac{T_m + T_M}{2}) \mathbf{E}_i^\top \mathbf{J}_a(\phi) \mathbf{K}_d \end{aligned} \quad (17)$$

where

$$\begin{aligned} \frac{\partial T}{\partial \mathbf{x}}(\mathbf{x}) &= \left[\frac{\partial T}{\partial q}(\mathbf{x}) \dot{\cdot} - \mathbf{J}_a(\phi) (\mathbf{K}_d + \boldsymbol{\mu}^{-1} \boldsymbol{\Gamma}_\zeta) \dot{\cdot} \right. \\ &\quad \left. \mathbf{J}_a(\phi) \boldsymbol{\mu}^{-1} \boldsymbol{\Gamma}_\zeta \dot{\cdot} \mathbf{J}_a(\phi) \dot{\cdot} \mathbf{J}_a(\phi) \mathbf{K}_p \dot{\cdot} \mathbf{J}_a(\phi) \mathbf{K}_d \right] \\ \frac{\partial T}{\partial q}(\mathbf{x}) &= -\mathbf{J}_a(\phi) \mathbf{K}_p - \left[\mathbf{0}_{3 \times 3} \dot{\cdot} \frac{\partial \mathbf{J}_a(\phi)}{\partial \phi_1} \mathbf{J}_a^{-1}(\phi) \mathbf{T}(\mathbf{x}) \dot{\cdot} \right. \\ &\quad \left. \frac{\partial \mathbf{J}_a(\phi)}{\partial \phi_2} \mathbf{J}_a^{-1}(\phi) \mathbf{T}(\mathbf{x}) \dot{\cdot} \frac{\partial \mathbf{J}_a(\phi)}{\partial \phi_3} \mathbf{J}_a^{-1}(\phi) \mathbf{T}(\mathbf{x}) \right]. \end{aligned}$$

with $\mathbf{J}_a(\phi) \triangleq \boldsymbol{\Xi}^{-1} \mathbf{B}^{-1}(\phi) \hat{\mathbf{M}}(\phi)$.

ACKNOWLEDGEMENT

The authors would like to thank Dohyun Eom (Seoul National University) for his help conducting the experiments.

REFERENCES

- [1] S. Kim, H. Seo, and H. J. Kim, "Operating an unknown drawer using an aerial manipulator," in *2015 IEEE international conference on robotics and automation (ICRA)*. IEEE, 2015, pp. 5503–5508.
- [2] D. Lee, H. Seo, D. Kim, and H. J. Kim, "Aerial manipulation using model predictive control for opening a hinged door," in *2020 IEEE International Conference on Robotics and Automation (ICRA)*. IEEE, 2020, pp. 1237–1242.
- [3] J. Byun, D. Lee, H. Seo, I. Jang, J. Choi, and H. J. Kim, "Stability and robustness analysis of plug-pulling using an aerial manipulator," in *2021 IEEE/RSJ International Conference on Intelligent Robots and Systems (IROS)*. IEEE, 2021, pp. 4199–4206.
- [4] Y. Sun, Z. Jing, P. Dong, J. Huang, W. Chen, and H. Leung, "A switchable unmanned aerial manipulator system for window-cleaning robot installation," *IEEE Robotics and Automation Letters*, vol. 6, no. 2, pp. 3483–3490, 2021.
- [5] E. Shahriari, S. A. B. Birjandi, and S. Haddadin, "Passivity-based adaptive force-impedance control for modular multi-manual object manipulation," *IEEE Robotics and Automation Letters*, vol. 7, no. 2, pp. 2194–2201, 2022.
- [6] T. Hui, E. Cuniato, M. Pantic, M. Tognon, M. Fumagalli, and R. Siegwart, "Passive aligning physical interaction of fully-actuated aerial vehicles for pushing tasks," in *2024 IEEE international conference on robotics and automation (ICRA)*. IEEE, 2024, pp. 6152–6158.
- [7] S. Hwang, D. Lee, C. Kim, and H. J. Kim, "Autonomous heavy object pushing using a coaxial tiltrotor," *IEEE Transactions on Automation Science and Engineering*, 2024.
- [8] B. Convens, K. Merckaert, M. M. Nicotra, R. Naldi, and E. Garone, "Control of fully actuated unmanned aerial vehicles with actuator saturation," *IFAC-PapersOnLine*, vol. 50, no. 1, pp. 12 715–12 720, 2017.
- [9] A. Afifi, M. van Holland, and A. Franchi, "Toward physical human-robot interaction control with aerial manipulators: Compliance, redundancy resolution, and input limits," in *2022 International Conference on Robotics and Automation (ICRA)*. IEEE, 2022, pp. 4855–4861.
- [10] M. Brunner, L. Giacomini, R. Siegwart, and M. Tognon, "Energy tank-based policies for robust aerial physical interaction with moving objects," in *2022 International Conference on Robotics and Automation (ICRA)*. IEEE, 2022, pp. 2054–2060.
- [11] F. Benzi, M. Brunner, M. Tognon, C. Secchi, and R. Siegwart, "Adaptive tank-based control for aerial physical interaction with uncertain dynamic environments using energy-task estimation," *IEEE Robotics and Automation Letters*, vol. 7, no. 4, pp. 9129–9136, 2022.
- [12] E. Cuniato, N. Lawrance, M. Tognon, and R. Siegwart, "Power-based safety layer for aerial vehicles in physical interaction using lyapunov exponents," *IEEE Robotics and Automation Letters*, vol. 7, no. 3, pp. 6774–6781, 2022.
- [13] D. Chaikalis and A. Tzes, "Optimization-based compliant controller for physical human-aerial manipulator interaction," in *2024 International Conference on Unmanned Aircraft Systems (ICUAS)*. IEEE, 2024, pp. 1325–1331.
- [14] D. Lee and H. J. Kim, "Saturated rise control for considering rotor thrust saturation of fully actuated multirotor," in *2024 International Conference on Unmanned Aircraft Systems (ICUAS)*. IEEE, 2024, pp. 39–44.
- [15] W. Ha and J. Back, "A disturbance observer-based robust tracking controller for uncertain robot manipulators," *International Journal of Control, Automation and Systems*, vol. 16, pp. 417–425, 2018.
- [16] A. Alan, T. G. Molnar, E. Daş, A. D. Ames, and G. Orosz, "Disturbance observers for robust safety-critical control with control barrier functions," *IEEE Control Systems Letters*, vol. 7, pp. 1123–1128, 2022.